7530 *Macromolecules* **2009**, *42*, 7530–7536
DOI: 10.1021/ma900667w

Macromolecules
ARTICLE

Influence of the Surface Field on the Self-Assembly of a Diblock Copolymer Melt Confined in a Cylindrical Nanopore

Weihua Li

The Key Laboratory of Molecular Engineering of Polymers Ministry of Education, China, Department of Macromolecular Science, Fudan University, Shanghai 200433, China

Robert A. Wickham*

Department of Physics, University of Guelph, Guelph, Ontario, Canada N1G 2W1

Received March 27, 2009; Revised Manuscript Received July 10, 2009

ABSTRACT: We study the influence of the surface field on lamellar morphologies that form in a diblock copolymer melt confined in a cylindrical nanopore, using self-consistent mean-field theory. By varying the pore diameter and surface field strength and by introducing a slight composition asymmetry, we systematically explore the stability regions of parallel and perpendicular lamellar phases and accurately compute the phase boundaries. When the surface field is weak, or the natural period of the lamellae is incommensurate with the pore size, lamellae perpendicular to the pore wall are preferred. A strong surface preference and/or a small composition asymmetry can lead to the formation of concentric parallel lamellae. In narrow pores, we find that complex structures can exist as equilibrium phases between regions of parallel and perpendicular lamellae. When we reduce the volume fraction of the block preferred by the pore wall, this composition asymmetry competes with the surface preference and can lead to the formation of perpendicular lamellae. This suggests a route to produce perpendicular lamellar phases in the common experimental situation where a surface preference is present. This competition also enables us to characterize the strength of the surface field in the theory.

I. Introduction

Self-assembly in block copolymer melts produces nanoscale structures that have potential applications as, for example, lithographic templates for nanowires, photonic crystals, or high-density magnetic storage media.[1] Novel nanostructures, beyond those seen in bulk samples, can form when the block copolymer melt is confined in nanoscale cavities created by solid boundaries. Confinement thus lends a rich physics to these systems, and the confinement of block copolymer melts, notably in cylindrical nanopores, has been the focus of much recent experimental[2−8] and theoretical[2,9−18] attention.

The interaction of the pore wall with the copolymer can favor having one monomer species closer to the wall than the others. In theory or simulation this interaction is represented by a surface field. Of all the factors that influence self-assembly under confinement—copolymer composition, interactions between different blocks, the size of the cavity, the curvature of the pore wall, and the surface field—it is the surface field that tends to be the least well-characterized aspect of the problem. In an experiment, the strength and range of the surface field are typically unknown, which makes precise comparison between experiment and theory difficult. Recent experiments that create cylindrical confinement through an electrospinning technique promise greater control of the surface field.[8] Our previous work used self-consistent mean-field theory (SCMFT) to explore the phase behavior of a cylindrically confined diblock copolymer melt as a function of the copolymer composition, the interactions between different blocks, and the diameter of the nanopore, but we did not consider the influence of the surface field in detail.[13,14] In this paper, we use SCMFT to systematically study the influence of the surface field on diblock copolymer melt self-assembly under cylindrical confinement. We restrict our attention to symmetric, or nearly symmetric, diblock copolymers, which form lamellae in the bulk. In this context, the influence of the surface field is straightforward to interpret. We do not address the interesting and difficult question of the functional form of the surface field; Monte Carlo simulations typically assume it is a contact interaction,[9,11,16,17] and we assume here that the surface field is a short-ranged, exponentially decaying function. Our focus centers on how the surface field strength, the incommensurability[19] of the pore diameter with the natural lamellar period, and the slight block asymmetry compete to determine microstructure formation.

Masten used SCMFT to study the interplay of the surface field with the incommensurability effect in the context of the slab geometry.[20] A similar study of the slab geometry, using SCMFT and Monte Carlo, was performed by Geisinger et al.[21] These systematic studies showed that there is a transition from lamellae perpendicular to the slab walls to lamellae parallel to the slab walls as the surface field is increased.

Melts of symmetric diblock copolymers confined in cylindrical nanopores have been studied previously. The curvature of the pore wall can shift the phase boundaries between parallel and perpendicular lamellae, compared to the slab case. Monte Carlo simulations by He et al.[9] demonstrated that concentric lamellar domains parallel to the pore wall ($L_{\parallel}$) form when the pore wall has a strong preference for one block. Dynamic density functional calculations of Sevink et al.[10] confirmed this observation and also revealed that perpendicular lamellae ($L_{\perp}$), oriented with their normals along the pore axis, are stable when the wall interaction is nonpreferential. Observing perpendicular lamellae in experiments is challenging since it is common to have a

*Corresponding author. E-mail: rwickham@physics.uoguelph.ca.

 Published on Web 09/04/2009

preferential wall. Symmetric polystyrene-*b*-polybutadiene (PS-*b*-PBD) copolymers confined in porous alumina formed concentric lamellar domains since the alumina pore wall had a preference for PBD.[3] Concentric lamellae were also observed in cylindrically confined polystyrene-*b*-poly(methyl methacrylate) copolymers[7] and in electrospun nanofibers with a copolymer core and a homopolymer shell.[8] Only when the pore size was decreased, so that the curvature imposed by the confinement became significant, were stacked disks (or tori) observed in the symmetric PS-*b*-PBD system.[4,6] This experimental work encouraged further study of cylindrically confined diblock copolymers by Monte Carlo simulation,[11,16,17] dissipative particle dynamics simulation,[12] and strong-segregation theory.[17] In addition to parallel and perpendicular lamellar morphologies, these studies revealed complex phases (helices, catenoid cylinder, gyroid) appearing under confinement, even for symmetric copolymers.[11,12,16,17] The Monte Carlo simulations of Feng and Ruckenstein[11] and of Chen et al.[16] explored the phase diagram as the pore diameter and surface field varied, although they were only able to examine a few points in the phase diagram. In a recent dynamic density functional study, Sevink et al.[18] went further in this direction. They examined the influence of the surface field and the pore diameter on the phase behavior of slightly asymmetric ($f = 0.45$) diblock copolymer melts confined in cylindrical nanopores. They demonstrated a $L_\perp$ to $L_\parallel$ transition with increasing surface field, and for narrow pores they found a region of stable catenoid cylinder phase; however, they found other complex, nonlamellar phases to be metastable. Their work suggests that incommensurability is playing a role in setting the $L_\perp/L_\parallel$ phase boundary, but they did not examine enough pore diameters to demonstrate this effect clearly.

An extensive, systematic study of surface field effects, which examines the balance between the surface field strength, the incommensurability effect, and the block asymmetry effect, is desirable. SCMFT is a successful approach to the problem of block copolymer self-assembly that has provided detailed information about bulk[22,23] and confined[13,14,20] phase behavior, and we employ it here. Our comprehensive examination of phase space enables us to precisely construct the phase boundary between the $L_\perp$ and $L_\parallel$ phases and to clearly see the behavior of the phase boundary as the pore diameter goes from being commensurate to incommensurate with the natural copolymer period. Differences with the earlier SCMFT work on the slab geometry[20] arise here due to the curvature of the pore walls. In narrow pores, we find that a perforated lamellar (catenoid cylinder) phase exists in equilibrium between regions of parallel and perpendicular lamellae. We demonstrate that a slight composition asymmetry can compete with a pore wall interaction preferential to the smaller block, stabilizing the $L_\perp$ phase. This highlights a route to create perpendicular lamellae in the common experimental situation where a preferential surface interaction is present. By making the surface field compete with incommensurability and with composition asymmetry, we are able to characterize the strength of the surface field in terms of observable effects on the morphologies that self-assemble. This will aid in the comparison of experiment to theory and also puts the surface field strength used in our previous work[13,14] into a broader context.

II. Theory

We consider an incompressible melt of AB diblock copolymers, confined to a cylindrical pore of diameter D. Each copolymer has a degree of polymerization N while the A-block on each has a degree of polymerization fN with $0 \le f \le 1$. Lengths in our theory are expressed in units of the radius of gyration of the polymer, R_g. Within the mean-field approximation to the many-chain Edwards theory,[24,25] at a temperature T the free energy F for n Gaussian diblock copolymer chains confined in a cylindrical pore has the following form:

$$\frac{F}{nk_BT} = -\ln Q + \frac{1}{V}\int_{|\mathbf{r}|\le R} d\mathbf{r}\Big\{\chi N\phi_A(\mathbf{r})\phi_B(\mathbf{r}) - \omega_A(\mathbf{r})\phi_A(\mathbf{r}) - \omega_B(\mathbf{r})\phi_B(\mathbf{r}) + H(\mathbf{r})[\phi_A(\mathbf{r}) - \phi_B(\mathbf{r})]\Big\} \quad (1)$$

The monomer densities are ϕ_A and ϕ_B; the partition function Q is for a single polymer interacting with the mean fields ω_A and ω_B produced by the surrounding chains. These quantities have the standard definitions and meanings.[22,23] The Flory−Huggins interaction parameter, χ, characterizes the repulsion between dissimilar monomers. In the confined melt, the spatial integration is restricted to the pore volume, taken to be V.

A surface field, $H(\mathbf{r})$, is included in eq 1 to describe the preference of the pore wall for either the A or B monomers. We assume that the surface field decays rapidly away from the pore wall, over the scale of a polymer coil. Following our previous work,[13,14] we choose the surface field to have the form (with $D = 2R$)

$$\frac{H(\mathbf{r})}{\chi N} = H_s\frac{\exp[(\sigma+|\mathbf{r}|-R)/\lambda]-1}{\exp(\sigma/\lambda)-1} \quad (2)$$

for $R - \sigma \le |\mathbf{r}| \le R$, while $H(\mathbf{r}) = 0$ for $|\mathbf{r}| < R - \sigma$. We choose the cutoff distance for the surface interaction to be $\sigma = 0.5R_g$ and the decay length to be $\lambda = 0.25R_g$. H_s is the strength of the surface field at the pore wall, in units of χN; this paper focuses on how variations in H_s influence the phase behavior. According to eqs 1 and 2, the pore wall has a preference for B monomers when $H_s > 0$ and a preference for A monomers when $H_s < 0$.

Minimization of the free energy, eq 1, with respect to the monomer densities and mean fields leads to the set of mean-field equations

$$\omega_A(\mathbf{r}) = \chi N\phi_B(\mathbf{r}) + H(\mathbf{r}) + \eta(\mathbf{r}) \quad (3)$$

$$\omega_B(\mathbf{r}) = \chi N\phi_A(\mathbf{r}) - H(\mathbf{r}) + \eta(\mathbf{r}) \quad (4)$$

$$\phi_A(\mathbf{r}) = \frac{1}{Q}\int_0^f ds\, q(\mathbf{r},s)q^\dagger(\mathbf{r},s) \quad (5)$$

$$\phi_B(\mathbf{r}) = \frac{1}{Q}\int_f^1 ds\, q(\mathbf{r},s)q^\dagger(\mathbf{r},s) \quad (6)$$

with

$$Q = \frac{1}{V}\int_{|\mathbf{r}|\le R} d\mathbf{r}\, q(\mathbf{r},s)q^\dagger(\mathbf{r},s) \quad (7)$$

Incompressibility

$$\phi_A(\mathbf{r}) + \phi_B(\mathbf{r}) = 1 \quad (8)$$

is enforced via the Lagrange multiplier $\eta(\mathbf{r})$, for $|\mathbf{r}| < R$. A key quantity appearing in these equations is the end-segment distribution function $q(\mathbf{r},s)$, which is proportional to the probability that a polymer chain segment, of contour length s and with one free end, has its other end located at $\mathbf{r}$. Both this distribution

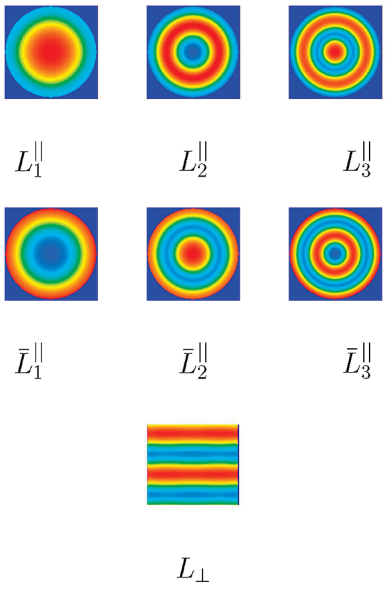

Figure 1. Typical monomer density distributions for the parallel ($L_n^{\parallel}$ and $\bar{L}_n^{\parallel}$) and perpendicular ($L_\perp$) lamellar phases that form in the pore. The pore axis coincides with the z axis. For the parallel phases, we show cross sections normal to the pore axis, while for the perpendicular phase we show a side view of the pore. Various pore radii and surface fields have been used to generate these structures. Domains of species A are blue, and the domains of species B are red. The subscript n denotes the number of concentric AB interfaces in the structure. An overbar means that the B block is in contact with the pore wall.

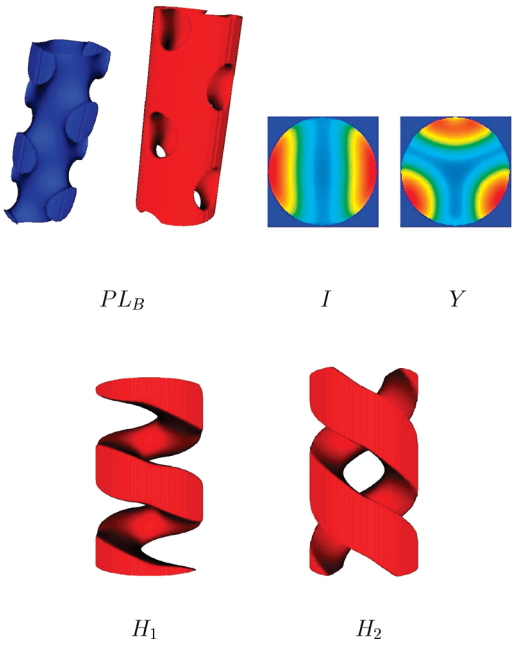

Figure 2. Typical monomer density distributions for complex structures that form in the pore. For the perforated layer (PL_B) structure we show the inner (A) domain (left, blue) and the outer (B) domain (right, red). The I and Y structures are translationally invariant along the pore, so we show only cross sections normal to the pore axis for these structures. Domains of species A are blue, and the domains of species B are red. The B domains of the single-helix (H_1) and double-helix (H_2) structures are shown.

function and its conjugate, $q^\dagger(\mathbf{r},s)$, satisfy the modified diffusion equations

$$\frac{\partial q(\mathbf{r},s)}{\partial s} = \nabla^2 q(\mathbf{r},s) - \omega(\mathbf{r},s) q(\mathbf{r},s) \tag{9}$$

$$-\frac{\partial q^\dagger(\mathbf{r},s)}{\partial s} = \nabla^2 q^\dagger(\mathbf{r},s) - \omega(\mathbf{r},s) q^\dagger(\mathbf{r},s) \tag{10}$$

with $\omega(\mathbf{r},s) = \omega_A(\mathbf{r})$ for $0 \le s \le f$ and $\omega(\mathbf{r},s) = \omega_B(\mathbf{r})$ for $f < s \le 1$. The initial conditions are $q(\mathbf{r},0) = 1$ and $q^\dagger(\mathbf{r},1) = 1$. Equations 3−10 can be solved self-consistently in real space to find the equilibrium densities.[22,23,26] We align the pore axis with the z-axis; the cross section of the pore is in the $x-y$ plane. We parallelize[27] the split-step Fourier method of Tzeremes et al.[28,29] to solve the modified diffusion equations for the end-segment distribution functions, using fast-Fourier transform (FFTW) libraries.[30] The diffusion equations are solved on a $N_x \times N_y \times N_z = 128 \times 128 \times 64$ cubic lattice, which our previous work[13,14] suggests is sufficiently large to produce accurate phase diagrams for the range of D we examine. This lattice is divided, along z, between up to eight processors. We impose periodic boundary conditions on all edges of the cubic lattice. The chain contour length for each block is discretized into 64 segments. Outside the pore there is no polymer, so we set the end-segment distribution functions to zero when $x^2 + y^2 \ge R^2$, which implies that $\phi_A = \phi_B = 0$ in this region. A recent study by Meng and Wang suggests that the phase behavior of confined diblock copolymers is not significantly influenced by the choice of the functional form for the vanishing density fields near the pore wall.[31] In the present case, we choose the density fields to vanish like a step function across one grid point near the pore wall. Our previous work[13] showed that halving the grid spacing changes the calculated free energy for a given structure but that the free energies of all structures change similarly, leading to only a minor effect on the computed phase boundaries. Thus, a variation of the range over which the density field vanishes at the pore wall does not significantly influence the phase behavior, consistent with the conclusion of ref 31. More details about our real-space calculations are given in ref 14.

We first use random initial conditions for the mean fields in our iterative algorithm to generate a set of solutions to the mean-field equations over a range of pore diameters, surface field strengths, H_s, and copolymer compositions, f. For each solution we find, we minimize the free energy of the structure with respect to variations of the length of the pore to eliminate extensional stress and to ensure that the pore length is commensurate with the natural period of the structure along z. Once we determine a set of solutions to the mean-field equations, we then use these solutions as initial conditions in our algorithm to explore the extent (if any) of their stability regions. We compute free energies to an accuracy of 1 part in 10^{-4}. We take the equilibrium phase to be the structure which has the lowest free energy, for a given D, H_s, and f, of all the structures we observe. This is a reasonable and necessary approach to construct the phase diagram since a method does not currently exist, within SCMFT, to directly identify the global minimum of the free energy.

III. Results and Discussion

We first consider a symmetric diblock copolymer ($f = 0.5$) with $\chi N = 15$. In the bulk, such a copolymer will form flat lamellar domains. Figure 1 displays the typical monomer density distributions that we observe when the copolymer is confined in a cylindrical nanopore. We use $L_n^{\parallel}$ to label the phase with concentric lamellae oriented parallel to the pore wall. The subscript n indicates the number of AB interfaces in the structure. An overbar ($\bar{L}_n^{\parallel}$) indicates that the B block is in contact with the pore wall. The phase with lamellae oriented perpendicular to the pore axis is denoted $L_\perp$.

In addition to parallel and perpendicular lamellae, we observe the complex structures shown in Figure 2. The perforated layer

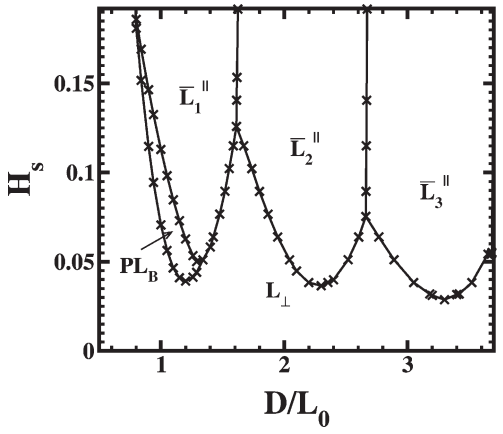

Figure 3. Phase diagram for fixed $f = 0.5$ and $\chi N = 15$, over a range of surface field strengths, H_s, and pore diameters, D. We scale the pore diameter in units of the bulk lamellar period, $L_0 = 3.71R_g$. The phases are labeled as in Figures 1 and 2. The crosses are calculated phase transition points, while the curves are guides to the eye, indicating the phase boundaries. The phase diagram is symmetric under $H_s \rightarrow -H_s$, with $L_n^{\parallel}$ replacing $\overline{L}_n^{\parallel}$ and PL_A replacing PL_B, when $H_s < 0$.

(PL_B) structure is a modified $\overline{L}_1^{\parallel}$ structure in which holes form in the outer circular lamellar B domain, allowing the inner A domain to penetrate the outer domain and come into contact with the pore wall (a PL_A structure would have the outer domain composed of the A block). Going along the pore axis, the arrangement of the holes alternate between two perpendicular axes. The *I* and *Y* structures, so named because of the appearance of the A domain in their cross section, are translationally invariant along the pore axis. Both are modified $\overline{L}_1^{\parallel}$ structures in which the outer circular lamellar B domain has broken up into 2 (*I*) and 3 (*Y*) domains. We also find single-helix (H_1) and double-helix (H_2) structures. We find that complex structures are usually metastable; however, in narrow pores the *PL* and *I* structures can become equilibrium phases in a region between the $L_{\perp}$ and $\overline{L}_1^{\parallel}$ phases.

In Figure 3, we plot the phase diagram for a range of $H_s > 0$ and D. The pore diameter is measured in units of the bulk lamellar period, $L_0 = 3.71R_g$, which we determine from a reciprocal-space SCFT calculation. When the surface field is neutral or only slightly preferential for the B block, the equilibrium phase is $L_{\perp}$. For an intermediate range of H_s, both parallel and perpendicular lamellae are possible, depending on D. Only the $\overline{L}_n^{\parallel}$ phases are equilibrium phases for sufficiently large H_s and D. In narrow pores ($0.8 \leq D/L_0 \leq 1.3$) the PL_B structure appears as an equilibrium phase in a narrow region between the $L_{\perp}$ and $\overline{L}_1^{\parallel}$ phases.

Figure 3 suggests that competition between the entropic penalty associated with chain stretching and the tendency of the surface field to favor the $\overline{L}_n^{\parallel}$ phase determine which structure forms in the pore. The $L_{\perp}$ phase is free to choose its period along the pore axis to minimize the chain stretching penalty. We find that the lamellar period selected in the $L_{\perp}$ phase is essentially L_0, independent of the parameters we examine. However, the $L_{\perp}$ structure has A domains in contact with the pore wall, which is unfavorable for $H_s > 0$. Thus, $L_{\perp}$ forms when H_s is small or at intermediate H_s when D is incommensurate with L_0 and the formation of concentric, parallel lamellae is unfavorable due to the high entropic penalties resulting from stretching the chains. The formation of perpendicular lamellae due to incommensurability, despite the presence of a surface preference, has been observed in experiments.[4,6] The $L_{\perp}$ phase also forms when D/L_0 is small, for all the H_s that we examine, because of incommensurability and also because of the unfavorable, high AB interfacial curvature that concentric lamellae would have in these narrow pores. The PL_B structure contains both protrusions of A domains perpendicular to the pore axis and an outer B layer that aligns parallel to the pore wall, suggesting that PL_B should be considered as intermediate between $L_{\perp}$ and $\overline{L}_1^{\parallel}$. In particular, this suggests that the average AB interfacial curvature of the PL_B structure is less than that for the $\overline{L}_1^{\parallel}$ structure. In a narrow pore, where confinement effects are strongest, the unfavorable, high AB interfacial curvature of the $\overline{L}_1^{\parallel}$ structure destabilizes $\overline{L}_1^{\parallel}$ in favor of the PL_B over a narrow region of the phase diagram. Large values of H_s favor having the B block completely coat the pore surface and will suppress both the $L_{\perp}$ and PL_B phases. For large H_s, as D increases, the system makes the direct transitions $\overline{L}_n^{\parallel} \rightarrow \overline{L}_{n+1}^{\parallel}$, adding one AB layer to relieve chain stretching. We observe that these layer-adding transitions are first-order transitions, in agreement with recent Monte Carlo simulations.[17] The locations of our $\overline{L}_1^{\parallel} \rightarrow \overline{L}_2^{\parallel}$ transition at $D/L_0 \approx 1.6$ and our $\overline{L}_2^{\parallel} \rightarrow \overline{L}_3^{\parallel}$ transition at $D/L_0 \approx 2.7$ are consistent with these Monte Carlo results.[17] The addition of concentric layers with increasing pore diameter has also been observed in experiments.[3,7,8]

The gross features of our phase diagram in Figure 3 are similar to those of the thin film geometry (Figure 7a of ref 20); however, there are some small, but notable, differences that arise due to the curvature of the pore wall in the present case. To begin, a perforated layer phase was not observed in ref 20. Furthermore, in the present work, the D for which the $\overline{L}_n^{\parallel}$ phase boundaries achieve a minimum in H_s do not occur at integer multiples of L_0, as in ref 20, but rather at a slightly larger values. The first three such minima are at $D/L_0 \approx 1.3$, $D/L_0 \approx 2.3$, and $D/L_0 \approx 3.3$. When the interfaces are curved, the block on the inside of the curvature must stretch more than it would when the interface is flat, and the block on the outside of the curvature is able to relax into a more coiled configuration. Our results suggest that the extra amount of stretching is slightly larger than the extra amount of coiling, leading to a most-preferred $\overline{L}_n^{\parallel}$ configuration in pores of slightly larger than integer D/L_0. Confinement-induced stretching of domains has been observed in experiments.[3] With decreasing D, the value of H_s at the minima in these phase boundaries increases slightly, whereas in ref 20 this value appears to be independent of D. Our observation suggests that the bending energy penalty to form curved concentric lamellae reduces the stability of the $\overline{L}_n^{\parallel}$ phase, with increased effect at smaller D (eventually leading to the presence of a PL_B phase in narrow pores). When $D/L_0 \gg 1$, we expect that the effects of pore curvature will be unimportant and that our phase diagram will approach that of the flat film case.[20] Previous numerical studies of cylindrically confined diblock copolymer melts also suggest that the stability region of the $L_{\perp}$ phase expands as D decreases.[11,18] The expanding stability regions for parallel lamellae with increasing D that we observe may explain why the Monte Carlo simulations of ref 11, with an A-monomer/surface interaction $\varepsilon_{AS} = -0.11k_BT$, observe perpendicular lamellae for $D/L_0 = 1.5$, but not for $D/L_0 = 2.5$, both ostensibly cases where D and L_0 are incommensurate. Indeed, the precision with which we locate the phase boundaries in Figure 3 leads to the observation that Figure 3, with $H_s \approx 0.06$, is consistent with the results of ref 11 for $\varepsilon_{AS} = -0.11k_BT$, where they observed a perpendicular lamellar phase for $D/L_0 = 1.5$ and parallel lamellar phases for $D/L_0 = 2$, 2.5, and 3.

In the Monte Carlo simulations of ref 17 the AB interfaces in the $L_{\perp}$ morphology were not flat when a preferential surface field was present. We also see this in our calculations. Figure 4 shows our monomer density profiles for the $L_{\perp}$ phase formed by a symmetric copolymer melt confined in a pore with $D/L_0 = 1.6$, for $H_s = 0$, $H_s = -0.064$, and $H_s = -0.128$. For $H_s = 0$ the AB interfaces are flat. As $|H_s|$ increases, so does the magnitude of the modulation of the AB interface, as the A block is preferred by the surface.

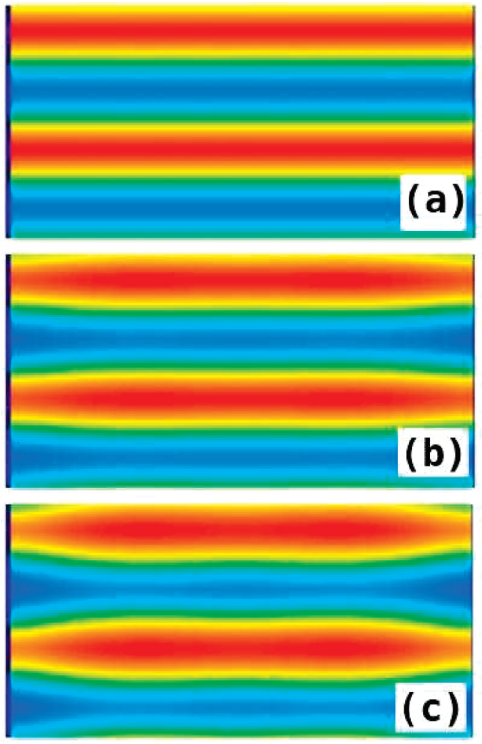

Figure 4. Monomer density profiles of the perpendicular phase formed in a symmetric diblock copolymer melt, confined in a pore with a fixed diameter $D/L_0 = 1.6$, for three values of surface fields: (a) $H_s = 0$, (b) $H_s = -0.064$, (c) $H_s = -0.128$. The side view of the pore is shown. Domains of species A are blue, and the domains of species B are red.

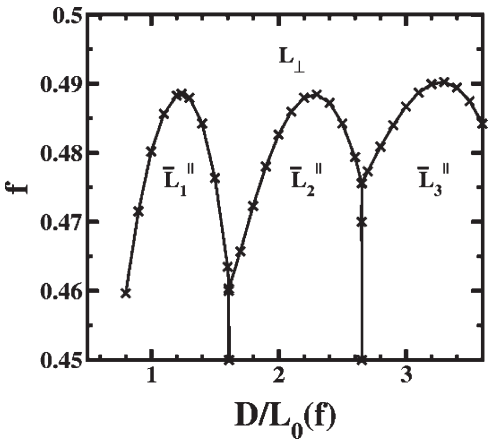

Figure 5. Phase diagram of block composition, f, vs pore diameter, D, for the case where the pore wall is neutral and $\chi N = 15$. The pore diameter is in units of the bulk lamellar period $L_0(f)$. L_0 is slightly dependent on f: L_0 increases from $3.70R_g$ at $f = 0.45$ to $3.71R_g$ at $f = 0.5$. The phases are labeled as in Figure 1. The crosses are calculated phase transition points, while the curves are guides to the eye, indicating the phase boundaries.

We now examine the influence of a slight composition asymmetry on the phase diagram for the simplest case of a neutral pore wall. In Figure 5 we plot the phase diagram for a range of copolymer compositions, $0.45 \le f \le 0.5$, and pore diameters. The pore diameter is measured in units of the bulk lamellar period, $L_0(f)$, which is weakly composition-dependent over the compositions we examine. Over this composition range and at this segregation, $\chi N = 15$, the lamellar phase is in equilibrium in the bulk, within SCMFT. The similarity of Figure 5 to Figure 3 suggests that composition asymmetry is playing a role similar to

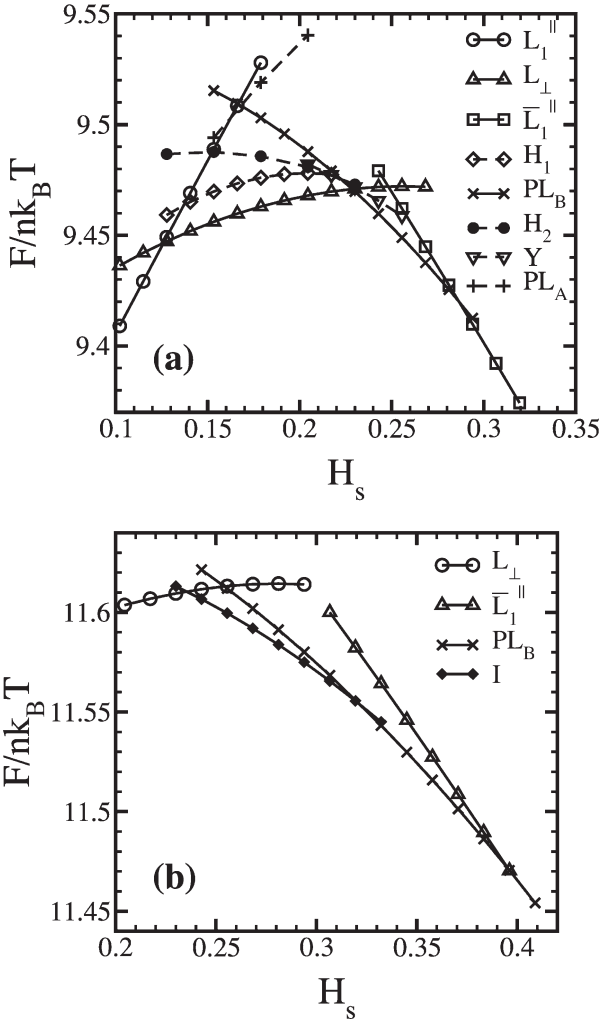

Figure 6. Comparison of the free energy F, eq 1, for various structures, with $f = 0.55$ and $\chi N = 15$, as a function of the surface field strength, H_s. The pore diameter, scaled in units of $L_0 = 3.70R_g$, is $D/L_0 = 1.4$ in (a) and $D/L_0 = 1$ in (b). The curve labels correspond to structures in Figures 1 and 2.

that of a surface field in the alignment of lamellar domains. For a small composition asymmetry, the equilibrium phase is $L_\perp$. On decreasing f, both parallel and perpendicular lamellae are possible, depending on D. Note that only a slight asymmetry is sufficient to influence the structure formation. Only the $\overline{L}_n^{\parallel}$ phases are equilibrium phases for sufficiently small f ($f \lesssim 0.47$) and sufficiently large D. These results suggest that the tendency for an asymmetric copolymer to form a curved AB interface, with the longer B block on the outside of the curvature, favors an equilibrium $\overline{L}_n^{\parallel}$ phase. As before, when D is incommensurate with L_0, perpendicular lamellae strongly compete with the tendency to form concentric, parallel lamellae. As in Figure 3, the phase boundaries achieve maxima in f at slightly greater than integer values of $D/L_0(f)$. In contrast to Figure 3, the PL_B structure is not an equilibrium phase in a narrow pore in Figure 5. Presumably, the tendency for an asymmetric copolymer to form a curved AB interface provides stability to the $\overline{L}_1^{\parallel}$ structure, favoring it over the PL_B structure, even in narrow pores.

Interestingly, our observation in Figure 5 (and later in Figure 7) that the longer block is in contact with the neutral pore wall contrasts with an argument, discussed in ref 31, that a flat neutral wall has an entropic preference for the shorter block of the diblock copolymer. Apparently, over the range of D we examine, the effect of the curvature of the pore wall favoring the larger

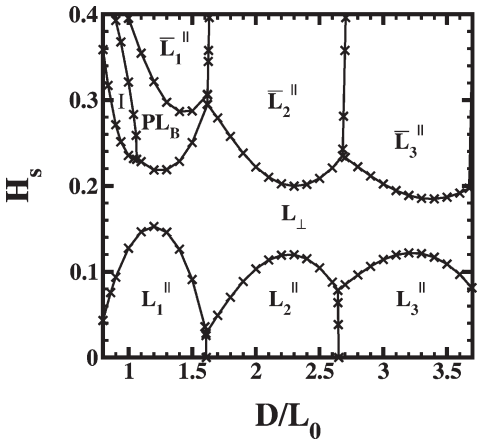

Figure 7. Phase diagram for a diblock copolymer with $f = 0.55$ and $\chi N = 15$ for a range of surface field strengths, H_s, and pore diameters, D. The pore diameter is scaled in units of $L_0 = 3.70R_g$. The phases are labeled as in Figures 1 and 2. The crosses are calculated phase transition points, while the curves are guides to the eye, indicating the phase boundaries.

block near the wall dominates this slight preference for the shorter block to be near the wall.

In Figure 6, we fix the copolymer composition to be $f = 0.55$ and focus on the surface field effect in the presence of this asymmetry, plotting the free energy for various structures over range of $H_s > 0$. Figure 6a, with $D/L_0 = 1.4$, shows the transition sequence $L_1^{\parallel} \rightarrow L_\perp \rightarrow PL_B \rightarrow L_1^{\parallel}$ as H_s increases. The helical H_1 and H_2 structures are metastable in Figure 6a but are nearly equilibrium at $H_s \approx 0.23$. Figure 6b, with $D/L_0 = 1$, displays the transition sequence $L_\perp \rightarrow I \rightarrow PL_B \rightarrow L_1^{\parallel}$ with increasing $H_s > 0.2$.

We use these results, and others, to create a phase diagram over a range of $H_s > 0$ and D, at fixed $f = 0.55$, shown in Figure 7. Since $f > 0.5$, the larger A block prefers to be on the outside of the curvature; thus, for a neutral pore wall, the $L_n^{\parallel}$ phases are in equilibrium, except at the smallest D. We find, however, that it is possible to form equilibrium $\overline{L}_n^{\parallel}$ phases, with the B block on the outside of the curvature, if the surface has a strong enough preference for the B block ($H_s > 0$). Between these two extremes, there is a region where the perpendicular lamellar phase is stable. The influence of the commensurability/incommensurability of the pore diameter with the natural period of the copolymer is evident.

In narrow pores in Figure 7 the I and PL_B structures appear as equilibrium phases between the $L_\perp$ and $\overline{L}_1^{\parallel}$ phases, consistent with the free energy curves in Figure 6. When $f = 0.55$, there is a tendency to curve the AB interface and put the A block on the outside of the curvature. This will stabilize the $L_1^{\parallel}$ phase and destabilize the $\overline{L}_1^{\parallel}$ phase (whose AB interfaces have the wrong sign for the curvature). The extra stability of the $L_1^{\parallel}$ phase may explain why the PL_A structure is not seen, and the reduced stability of the $\overline{L}_1^{\parallel}$ phase may be responsible for the existence of equilibrium I and PL_B phases in narrow pores in Figure 7. There is no region in any of our phase diagrams (Figures 3, 5, or 7) where helical structures are in equilibrium.

Figure 7 reveals a competition between the tendency of the system to form curved AB interfaces with the larger A block on the outside of curvature and the opposing tendency of the surface field to attract the B block to the pore wall. Thus, we can use Figure 7 to quantify the strength of the surface field, relative to the energy scale for the formation of spontaneous curvature. Weak surface fields ($H_s \lesssim 0.1$) cannot overcome the spontaneous curvature effect, while strong surface fields ($H_s \gtrsim 0.2$) can. This suggests that the surface field $H_s = 1 - e^{-2} \approx 0.86$ we used in our previous work[14] was strongly aligning, at least relative to the energy scale to generate spontaneous curvature when $f = 0.55$. Another interesting consequence of Figure 7 is that it reveals that it is possible to form a perpendicular phase even in the presence of a surface field strength $H_s \approx 0.18$, if the surface field and spontaneous curvature effects balance. For the symmetric copolymer in Figure 3, such a surface field strength would produce a parallel phase. This suggests a practical method to create perpendicular lamellar phases in nanopores in the common situation of a preferential pore wall by using composition asymmetry.

Our observation of transitions from perpendicular to parallel lamellar structures with increasing surface field strength is consistent with previous numerical studies.[10−12,16−18] Most of these studies, however, have only examined a small set of points in the parameter space of pore diameter versus surface field preference, in part due to the extensive resources required for these simulations. Experimental studies are similarly limited since the surface field strength is fixed by the choice of copolymer and pore wall material, typically alumina.[3,7] However, recent experiments using electrospun polymer nanofibers with a copolymer core and a glassy polymer shell hold the promise of allowing for variation of the copolymer/wall interaction through the use of different polymer shell materials.[8]

The recent dynamic density functional study of Sevink et al. systematically examined the parameter space for this system.[18] Indeed, their Figure 7, using a slightly asymmetric diblock copolymer with $f \approx 0.45$, has similar features to our Figure 7. One significant difference, however, is that they observe a $L_\perp$ structure when the pore wall is neutral, whereas we observe that $L_n^{\parallel}$ phases are stable in this instance, as we discuss above. It may be that the short ($N = 22$) polymers used in the dynamic density functional theory result in an underestimation of the strength of the entropic effect leading to the spontaneous curvature of the AB interface. Whereas ref 18 examines a single $f \approx 0.45$, we examine a range of composition asymmetries as we show in Figure 5, and this figure demonstrates that only a small asymmetry is sufficient to stabilize concentric parallel lamellae. Our study examines the surface field strength/pore diameter parameter space with more resolution than previous studies. We precisely locate the phase boundaries for perpendicular-to-parallel transitions and for transitions between parallel structures with different numbers of layers. The phase diagram is shaped by the effects of incommensurability of the pore diameter with the natural lamellar period. Our work clearly reveals such effects, which were suggested in Figure 7 of ref 18.

Other groups, employing Monte Carlo[11,16,17] and dynamic density functional theory,[18] observed a perforated layer structure (often called a catenoid cylinder) in symmetric and slightly asymmetric block copolymers, similar to what we observe here. In work where the parameter space has been explored,[11,16,18] the perforated layer structure appears in narrow pores as an intermediate structure between perpendicular and parallel lamellae. This agrees with our observations. Figure 7 of ref 18 has a perforated layer phase on either side of the $L_\perp$ phase window, in contrast with our Figure 7, where we observe only the PL_B structure. References 11 and18 observed structures similar to our I structure, although Figure 7 of ref 18 does not exhibit an equilibrium I phase. The dynamic density functional study of ref 18 found helical structures to be metastable, in agreement with our observations. In this study, we adjust the pore length to minimize the free energy, which zeros any extensional forces. These extensional forces were difficult to eliminate in previous studies and can also lead to the formation of helical structures, as discussed in refs 17 and 18. Our present study, in which we compute the free energy of each observed structure, provides further evidence for the metastability of helical structures previously observed in Monte Carlo[11,16] and dissipative particle dynamics simulations[12] of cylindrically confined symmetric diblock copolymers.

To summarize, we used SCMFT to perform an extensive, systematic study of surface field effects in cylindrically confined diblock copolymer melts. We explored the interplay of the surface field, the incommensurability between the pore diameter and the natural lamellar period, and the copolymer composition asymmetry on the formation of microstructure. As seen previously, there is a transition from perpendicular to parallel lamellae with increasing surface field strength; however, our comprehensive study allows us to accurately plot the phase boundaries and to clearly see how the incommensurability of the pore diameter with the natural copolymer period influences the stability of these structures. Over the parameters we examine, we find parallel or perpendicular lamellae to be the dominant equilibrium phases; however, in narrow pores the PL_B and I structures can become equilibrium phases in a region between the $L_\perp$ and $\overline{L}_1^{\parallel}$ phases. We performed a systematic study of the effect of composition asymmetry on self-assembly in this work. For neutral or weak surface fields, the spontaneous curvature of the AB interface, induced by only a slight composition asymmetry, will favor the formation of concentric lamellae with the majority block on the outside of the curvature, nearest to the pore wall. However, if a surface field that favors the smaller block is applied, we found that we can reverse this situation, if the field is strong enough, and have the smaller block situate near the surface. When the opposing tendencies of this surface field and the spontaneous interfacial curvature balance, a perpendicular phase is found in equilibrium. We can characterize the strength of the surface field by balancing the surface field energy with the energy scale to form spontaneous curvature for a given composition asymmetry. Our finding of an equilibrium perpendicular lamellar phase when there is a significant surface preference suggests a route to produce such phases via composition asymmetry in the situation commonly encountered experimentally—that of a preferential surface field.

Acknowledgment. This work was initiated at St. Francis Xavier University in Antigonish, Nova Scotia, and the authors gratefully acknowledge the StFX hpcLAB and Greg Lukeman for computing resources and support. Further computing resources were provided by SHARCNET and by the High-End Computing Centre at Fudan University. W. Li gratefully acknowledges support in the early stages of this work from Professor D. Hunter and from the NSERC Research Capacity Development in Small Universities program. This work was also supported by CFI, the National Science Foundation of China (Grant No. 20704010), and the Shanghai Pujiang Program (Program No. 08PJ1402000).

References and Notes

(1) Park, C.; Yoon, J.; Thomas, E. L. *Polymer* **2003**, *4*, 6725–6760.
(2) Wu, Y.; Cheng, G.; Katsov, K.; Sides, S. W.; Wang, J.; Tang, J.; Fredrickson, G. H.; Moskovits, M.; Stucky, G. D. *Nat. Mater.* **2004**, *3*, 816–822.
(3) Xiang, H.; Shin, K.; Kim, T.; Moon, S. I.; McCarthy, T. J.; Russell, T. P. *Macromolecules* **2004**, *37*, 5660–5664.
(4) Shin, K.; Xiang, H.; Moon, S. I.; Kim, T.; McCarthy, T. J.; Russell, T. P. *Science* **2004**, *306*, 76.
(5) Xiang, H.; Shin, K.; Kim, T.; Moon, S. I.; McCarthy, T. J.; Russell, T. P. *Macromolecules* **2005**, *38*, 1055–1056.
(6) Xiang, H.; Shin, K.; Kim, T.; Moon, S. I.; McCarthy, T. J.; Russell, T. P. *J. Polym. Sci., Part B: Polym. Phys.* **2005**, *43*, 3377–3383.
(7) Sun, Y.; Steinhart, M.; Zschech, D.; Adhikari, R.; Michler, G. H.; Gösele, U. *Macromol. Rapid Commun.* **2005**, *26*, 369–375.
(8) Ma, M.; Krikorian, V.; Yu, J. H.; Thomas, E. L.; Rutledge, G. C. *Nano Lett.* **2006**, *6*, 2969–2972.
(9) He, X.; Song, M.; Liang, H.; Pan, C. *J. Chem. Phys.* **2001**, *114*, 10510–10513.
(10) Sevink, G. J. A.; Zvelindovsky, A. V.; Fraaije, J. G. E. M.; Huinink, H. P. *J. Chem. Phys.* **2001**, *115*, 8226–8230.
(11) Feng, J.; Ruckenstein, E. *Macromolecules* **2006**, *39*, 4899–4906.
(12) Feng, J.; Liu, H.; Hu, Y. *Macromol. Theory Simul.* **2006**, *15*, 674–685.
(13) Li, W.; Wickham, R. A.; Garbary, R. A. *Macromolecules* **2006**, *39*, 806–811.
(14) Li, W.; Wickham, R. A. *Macromolecules* **2006**, *39*, 8492–8498.
(15) Yu, B.; Sun, P.; Chen, T.; Jin, Q.; Ding, D.; Li, B.; Shi, A.-C. *Phys. Rev. Lett.* **2006**, *96*, 138306−1–4.
(16) Chen, P.; He, X.; Liang, H. *J. Chem. Phys.* **2006**, *124*, 104906−1–6.
(17) Wang, Q. *J. Chem. Phys.* **2007**, *126*, 024903−1–11.
(18) Sevink, G. J. A.; Zvelindovsky, A. V. *J. Chem. Phys.* **2008**, *128*, 084901−1–16.
(19) When the pore diameter is near to an integer multiple of the natural lamellar period, we refer to the situation as "commensurate". When the pore diameter is near to a half-integer multiple of the natural lamellar period, we refer to the situation as "incommensurate".
(20) Matsen, M. W. *J. Chem. Phys.* **1997**, *106*, 7781–7791.
(21) Geisinger, T.; Müller, M.; Binder, K. *J. Chem. Phys.* **1999**, *111*, 5241–5250.
(22) Matsen, M. W.; Schick, M. *Phys. Rev. Lett.* **1994**, *72*, 2660–2663.
(23) Masten, M. W. *J. Phys.: Condens. Matter* **2002**, *14*, R21–R47.
(24) Helfand, E. *J. Chem. Phys.* **1975**, *62*, 999–1005.
(25) Hong, K. M.; Noolandi, J. *Macromolecules* **1981**, *14*, 727–736.
(26) Drolet, F.; Fredrickson, G. H. *Phys. Rev. Lett.* **1999**, *83*, 4317–4320.
(27) Sides, S. W.; Fredrickson, G. H. *Polymer* **2003**, *44*, 5859–5866.
(28) Tzeremes, G.; Rasmussen, K. Ø.; Lookman, T.; Saxena, A. *Phys. Rev. E* **2002**, *65*, 041806−1–5.
(29) Rasmussen, K. Ø.; Kalosakas, G. *J. Polym. Sci., Part B: Polym. Phys.* **2002**, *40*, 1777–1783.
(30) Frigo, M.; Johnson, S. G. FFTW: an adaptive software architecture for the FFT. *Proc. ICASSP 1998* **1998** (3), 1381−1384.
(31) Meng, D.; Wang, Q. *J. Chem. Phys.* **2007**, *126*, 234902−1–10.